Ionization-induced laser-driven QED cascade in noble gases

I. I. Artemenko and I. Yu. Kostyukov*

Institute of Applied Physics, Russian Academy of Science, 46 Uljanov Strasse, 603950 Nizhny Novgorod, Russia

(Received 31 July 2017; published 6 September 2017)

A formula for the ionization rate in an extremely intense electromagnetic field is proposed and used for numerical study of QED cascades in noble gases in the field of two counterpropagating laser pulses. It is shown that the number of the electron-positron pairs produced in the cascade increases with the atomic number of the gas, where the gas density is taken to be inversely proportional to the atomic number. While most of the electrons produced in the laser pulse front are expelled by the ponderomotive force from the region occupied by the strong laser field, there is a small portion of electrons staying in the laser field for a long time until the instance when the laser field is strong enough for cascading. This mechanism is relevant for all gases. For high-Z gases there is an additional mechanism associated with the ionization of inner shells at the instance when the laser field is strong enough for cascading. The role of both mechanisms for cascade initiation is revealed.

DOI: 10.1103/PhysRevA.96.032106

I. INTRODUCTION

Recently, QED cascades in a strong laser field have attracted much attention [1–3]. The upcoming laser facilities will be able to generate laser pulses with a total power up to 10 PW [4,5]. It is generally believed that such power can be sufficient to observe QED cascading in laboratory conditions [6–8]. A cascade develops as a sequence of elementary QED processes: photon emission by electrons and positrons in the laser field alternates with pair production as a result of interaction between a high-energy photon and laser photons (Breit-Wheeler process [9]). Such a sequence leads to avalanchelike production of electron-positron plasma and γ rays. The number of cascade particles can be so great that they will affect the laser field dynamics. In particular, the laser field can be absorbed in self-generated plasma [10,11].

Several configurations of the laser field are proposed to minimize laser power needed for cascading. One of the simplest configurations is the superposition of two counterpropagating laser pulses. It is shown [12] that the linear polarization of laser radiation is more favorable for cascading than a circular one in the low-intensity limit. The laser-dipole wave can provide development of a QED cascade at laser power below 10 PW [8]. A field structure which is very similar to the dipole wave can be formed by 12 laser pulses [13]. Another laser configuration providing QED cascading at a power level below 10 PW can be constructed by coherent summation of several laser pulses with elliptical polarization [6]. The focal spot size has crucial importance for QED cascading [7]. On the one hand, by reducing the size of the focal spot at a given power it is possible to increase the intensity of the laser field, thereby increasing the probability of QED processes. On the other hand, if the spot size is not large enough, the cascade particles may escape quickly from the cascade volume, thereby suppressing cascade development.

In the high-intensity limit the cascade can be initiated by the spontaneous creation of electron-positron pairs out of vacuum (self-seeded QED cascades) [10]. In the low-intensity limit and near the intensity threshold, the seed particles are needed to trigger cascading. The seeded particles can be either electrons [6,11,12] or high-energy photons [14]. The electrons as light particles can be expelled from the cascade region by the ponderomotive potential of the laser field before the field strength reaches a maximum, and only a small portion of the seed electrons may survive to trigger a cascade [12]. Expulsion of the highly relativistic electrons by the ponderomotive force is suppressed due to the relativistic gain in the electron mass [15]. Yet the use of relativistic electrons as seed particles is hindered by the high cost of high-energy electron accelerators. In addition this also requires focusing of the electrons on the interaction region and synchronization between the electron beam and laser pulses. The same reasons (high cost of bright γ-ray sources, focusing and synchronization of the γ beam) may prevent the use of high-energy photons as seed particles.

Gases with high-Z atoms can be a source of seed electrons. The ionization potential of the inner electrons of high-Z atoms can be so large that such electrons can leave the atoms at very high laser field strength. Therefore the seed electrons can be produced by field ionization when the laser field strength peaks and is strong enough for cascading. It was demonstrated recently [7] that cascade triggering in the field of two counterpropagating laser pulses may be facilitated by employing suitable high-Z gases. However, the simplified model for atom ionization was used, and only hydrogen and oxygen are explored for the gas target. The model does not take into account the probabilistic nature of ionization, the dependence of the ionization probability on the shell electron parameters, or the sequential and multiple ionization of high-Z atoms. As a result, this model cannot provide an accurate description of the ionization and the dynamics of the seed electrons. In our work QED cascading in all noble gases irradiated by counterpropagating laser pulses is studied by three-dimensional particle-in-cell Monte Carlo (3D PIC-MC) simulations with a more realistic approach to laser ionization. We propose an ionization-rate formula that extends the known formula for tunnel ionization [16,17] to extremely intense field when the potential barrier is strongly suppressed.

It should be noted that the foils made from a high-Z material can also be used as a laser target and the source of the seeded electrons [18]. However, because of large target density QED cascade development can be affected by collisional processes

*kost@appl.sci-nnov.ru

like bremsstrahlung and electron-positron pair production as a result of photon scattering by nuclei. Here we discuss the use of rarified gases in order to neglect collisional processes.

This paper is organized as follows. The field-ionization model is described in Sec. II. In Sec. III, the results of 3D PIC simulations of QED cascades are presented. The distribution and the spectrum of the cascade particles are calculated. Section VI contains a discussion and conclusions. The contribution of collisional effects is estimated and discussed.

II. IONIZATION MODEL

The effect of a strong electromagnetic field on an atom may lead to ionization. In the tunnel regime of ionization the atom's electrons penetrate through the potential barrier formed by the atomic field and the external electric field. At low intensities the field ionization occurs in the multiphoton regime. The regime of the field ionization depends on the Keldysh parameter $\gamma_K = a^{-1}(2I_i/m_ec^2)^{1/2}$, where I_i is the ionization potential of the ion, $a = eE_L/(m_ec\omega_L)$ is the dimensionless laser field, E_L and ω_L are the laser field strength and the laser frequency, respectively, e and m_e are the charge and mass of the electron, respectively, and c is the speed of light [19]. It is generally believed that the field ionization occurs in the tunnel regime if $\gamma \lesssim 0.5$ [20]. In our simulations the electromagnetic field can be treated as static within the code time step. The rate of ionization in the static electric field is in the tunnel regime [16,17,21]:

$$W_{TI} = \omega_a\kappa^2 C_{kl}^2\left(\frac{2}{F}\right)^{2n^*-m-1} \times \frac{(l+m)!(2l+1)}{2^m m!(l-m)!}\exp\left(-\frac{2}{3F}\right),$$
$$C_{kl}^2 = \frac{2^{2n^*}}{n^*\Gamma(n^*+l^*+1)\Gamma(n^*-l^*)}, \quad (1)$$

where $F = E/(\kappa^3 E_a)$ is the normalized electric field, $n^* = Z/\kappa$ is the effective principal quantum number of the ion, Z is the ion charge number, $\kappa^2 = I_i/I_H$, $I_H = m_ee^4/(2\hbar^2) \simeq 13.59843\,\mathrm{eV}$ is the ionization potential of hydrogen, $l^* = n^* - 1$ is the effective angular momentum, l and m are the orbital and magnetic quantum numbers, respectively, $E_a = m_e^2e^5\hbar^{-4} \approx 5.14224 \times 10^9\,\mathrm{V/cm}$ is the atomic electric field, $\omega_a = m_ee^4\hbar^{-3} \simeq 4.13 \times 10^{16}\,\mathrm{s}^{-1}$ is the atomic frequency, $\hbar$ is the Planck constant, and $\Gamma(x)$ is the gamma function [22]. In the limit $n^* \gg 1$ formula (1) reduces to the ionization rate given in Ref. [23].

Formula (1) is valid when the unperturbed atomic energy level is much lower than the potential barrier maximum. This condition is fulfilled when the external field strength is much less than the critical field $E \ll E_{cr} = E_a\kappa^4/(16Z)$ [24]. For hydrogenlike atoms and ions with regard to the Stark effect $E_{cr,H} = (2^{1/2}-1)E_a$ [25]. We will use the expression $E_{cr} = E_a\kappa^4/(16Z)$ because $E_{cr} < E_{cr,H}$ and the ionization rate given by W_{TI} strongly deviates from the results of numerical simulations for $E > E_{cr}$ [26].

The barrier-suppression regime of the field ionization is relevant if $E > E_{cr}$. The analytical description of this regime is difficult since the perturbation methods are no longer valid for $E \sim E_{cr}$. For example, the analytical formula derived in Ref. [27] for the field-ionization rates in the barrier-suppression regime does not agree with numerical time-dependent Schrödinger equation (TDSE) calculations for $E > E_{cr}$ [28].

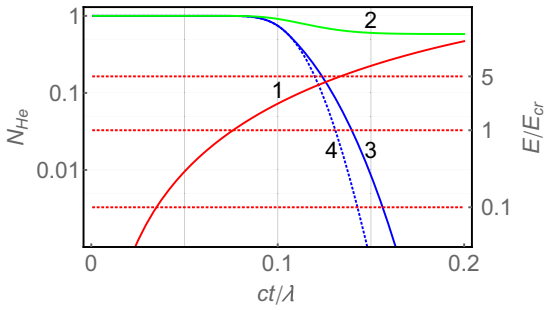

FIG. 1. The dependence of the laser field strength on time (line 1) and the probabilities of He not to be ionized as a function of time (lines 2–4). The probabilities are calculated by integrating W_{TI} (line 4), W_{PW} (line 3), and the ionization rate proposed in Ref. [26] (line 2) over time.

Several empirical formulas based on numerical simulations have been proposed for the ionization rate in the tunnel and barrier-suppression regimes [26,28,29]. In Ref. [28] the piecewise formula for ionization rate is proposed so that W_{TI} is used for $E \leqslant E_{TIQ} \sim E_{cr}$ while the quadratic dependence of the rate on the field strength is assumed for $E > E_{TIQ}$,

$$W_Q(E) = \omega_a 2.4(E/E_a)^2, \quad (2)$$

where E_{TIQ} is a threshold electric field determined by requiring $W(E)$ to be continuous, $W_{TI}(E_{TIQ}) = W_Q(E_{TIQ})$. Other empirical formulas providing a continuous transition between tunnel and barrier-suppression regimes are presented in Refs. [26,29].

The proposed formulas for the ionization rate become inaccurate in the limit of the extremely high field. For example, according to numerical TDSE simulations the dependence of the ionization rate on the field strength is close to linear rather than quadratic for $E > 0.4E_a \gg E_{cr}$ [28]. The formula proposed in Ref. [26] predicts a reduction in the ionization rate in the limit $E \gg E_{cr}$ that does not agree with numerical simulations [29]. However, the ionization-rate formula, which is valid for $E \gg E_{cr}$, is needed to analyze field ionization for a laser intensity above $10^{23}\,\mathrm{W/cm^2}$ when QED cascading is possible. For example, Eq. (1) for tunnel ionization predicts that 90% ionization of He in the electric field

$$E(t) = a\frac{mc\omega_L}{e}\sin(\omega_L t)\sin^2\left(\frac{t}{T}\right) \quad (3)$$

occurs when the laser field strength achieves the value $E \approx 4E_{cr}$ (see Fig. 1), where $0 \leqslant t \leqslant 20\lambda/c$, $a = 500$, $\omega_L = 2\pi c/\lambda$, $T = 40\omega_L c$, and $\lambda = 1\ \mu\mathrm{m}$ is the laser wavelength. The probability for He not to be ionized can be calculated as follows: $P(t) = 1 - \exp\{-\int_{-\infty}^{t} W_{TI}[|E(\tau)|]d\tau\}$. The ionization rate given by Eq. (1) is greater than that numerically calculated for $E \gg E_{cr}$ [26,28]. Therefore the 90% ionization of He will be achieved even at fields higher than $4E_{cr}$.

In the limit of an extremely strong laser field the ion field can be neglected, and the electrons inside the ion can be considered unbound just after the laser field is turned on quickly. The field of the ion with charge Z at the position of the outer electron can be estimated as $E_i(r_0) \simeq eZ/r_0^2 = 16E_{cr}$ at the beginning of ionization, where $r_0 \simeq a_B Z/\kappa^2 = 4r_m(E_{cr})$ is the orbit radius of the electron with ionization potential I_i, $r_m(E) = (eZ/E)^{1/2}$ is the position of the potential barrier maximum for the electron in the ion field and the external electric field E, and $a_B = \hbar^2/(m_e c^2)$ is the Bohr radius. Therefore the ion field can be neglected if $E \gg 16E_{cr}$. However, $16E_{cr}$ is the maximum value of the ion field that an electron feels during ionization. The condition for neglecting of the ion field can be taken as $E \gg E_{cr}$ because in this limit the ionization energy is much higher than the potential barrier maximum.

The ionization time can be estimated from a model of a free electron as the time needed to accelerate the electron from the energy of the atomic level $\varepsilon_e = -I_i$ to the continuum $\varepsilon_e = 0$ so that $I_i = m_e c^2[(1 + a^2\omega_L^2\tau_i^2)^{1/2} - 1]$, where ε_e is the electron energy, τ_i is the ionization time, and $amc\omega_L/e = E$ is the external electric field accelerating the electron. Therefore the ionization rate in the limit of extremely strong field can be estimated as follows: $W_L \approx \tau_i^{-1} = \omega_L a[(1 + I_i/m_e c^2)^2 - 1]^{-1/2}$. Neglecting the relativistic corrections ($I_i \ll m_e c^2$), we get the linear dependence of the rate on the electric field,

$$W_L(E) \approx \omega_L a\sqrt{\frac{m_e c^2}{2I_i}} = \omega_a \frac{E}{E_a}\sqrt{\frac{I_H}{I_i}}. \tag{4}$$

Finally, making use of a piecewise approach, the formula for the field-ionization rate can be extended to the limit of extremely strong field when the potential barrier is strongly suppressed,

$$W_{PW}(E) = \begin{cases} W_{TI}(E), & \text{if } E \leqslant E_{TIL}, \\ W_L(E), & \text{if } E > E_{TIL}, \end{cases} \tag{5}$$

where E_{TIL} is a threshold electric field and a solution of the transcendent equation $W_{TI}(E) = W_L(E)$.

It is interesting to note that, according to our calculation, the intersection between $W_{TI}(E)$ and $W_L(E)$ occurs at a reasonable field strength $E_{TIL} \sim E_{cr}$ for all noble gases. For example, for all 54 electrons of Xe, $1.15E_{cr} < E_{TIL} < 1.91E_{cr}$. If the last two electrons ($1s^1$ and $1s^2$ electrons) of Xe are excluded, then $1.15E_{cr} < E_{TIL} < 1.45E_{cr}$. The formula proposed in Ref. [28] as a combination of $W_{TI}(E)$ and $W_Q(E)$ predicts an unphysical value of the threshold electric field $E_{TIQ} = 0$ for ionization of the $1s^2$ electron of He [see Fig. 2(a)]. It is worth noting that $W_Q(E)$ for hydrogen starts to significantly deviate from numerical results at $E = E_{QL} \simeq 0.4E_a$, where $W_Q(E)$ crosses $W_L(E)$ [see Fig. 6 in Ref. [28] and Fig. 2(b)].

In order to take into account the multiple ionizations within one time step of the PIC code the MC kinetic numerical model is used [30]. The method is based on the solution of the set of coupled first-order differential equations describing evolution of the ion charge state [31]. The equations can be solved numerically [32,33] or analytically [30], assuming that the field distribution and the ionization probabilities do not change within the time step. Ionization events are modeled by MC numerical scheme as a random process in which the ionization rate is determined by Eq. (5). The energy losses because of ionization are neglected as they are much less than the losses associated with QED cascading (see Sec. IV).

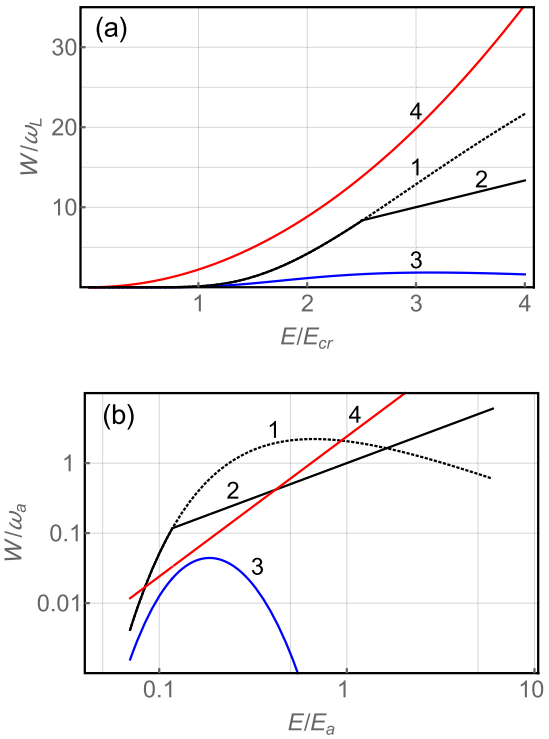

FIG. 2. (a) The ionization rates $W_{TI}(E)$ (line 1), $W_{PW}(E)$ (line 2), and W_Q (line 4) and the rate proposed in Ref. [26] (line 3) as functions of the field strength for single-electron ionization of He. (b) The ionization rates $W_{TI}(E)$ (line 1), $W_{PW}(E)$ (line 2), and W_Q (line 4) and the rate proposed in Ref. [26] (line 3) as functions of the field strength for ionization of hydrogen.

III. NUMERICAL SIMULATIONS

Development of a laser-assisted QED cascade in noble gases is studied by 3D PIC-MC simulations with the code QUILL [11,34]. The part of the code based on PIC method models the dynamics of a plasma and laser field, while the part based on the MC method models the emission of high-energy photons, electron-positron pair creation, and field ionization of atoms and ions.

In our simulations two laser pulses propagate towards each other along the x axis (see Fig. 3). The laser pulse

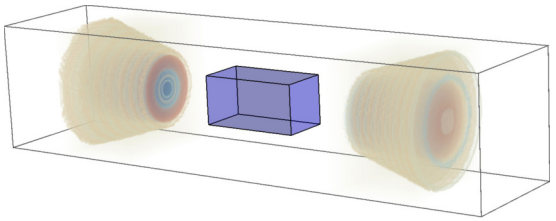

FIG. 3. The scheme of the laser pulse interaction with gas volume. Two counterpropagating laser pulses are focused on the gas-volume center.

centers are located at the points $x_0 = 16\lambda$, $y_0 = z_0 = 16.5\lambda$ and $x_0 = 40\lambda$, $y_0 = z_0 = 16.5\lambda$ at $t = 0$, respectively, where $\lambda = 1$ μm. The pulses are focused on the point $x_c = 28\lambda$, which is the center of the gas volume. The laser pulses have linear polarization ($E_z = B_y = 0$), and the y component of the electric field at $t = 0$ is

$$
\begin{aligned}
E_y(\mathbf{r}) &= A(\mathbf{r})\cos^2\left[\frac{\pi\sqrt{y^2+z^2}}{2\sigma(\mathbf{r})}\right]\Upsilon(\mathbf{r}),\\
\Upsilon(\mathbf{r}) &= \cos^2\frac{\pi x}{2\sigma_x}\cos\psi(\mathbf{r}) - \frac{\lambda}{4\sigma_x}\sin\psi(\mathbf{r})\sin\frac{\pi x_s}{\sigma_x},\\
\psi(\mathbf{r}) &= R(\mathbf{r}) - \arctan\frac{d}{x_R} - \arctan\frac{x_s - d}{x_R},\\
R(\mathbf{r}) &= k_L\left[x_s + \frac{(y^2+z^2)(x_s-d)}{2(x_s-d)^2 + 2x_R^2}\right],\\
x_s &= x - x_0,\\
\sigma(\mathbf{r}) &= \frac{\pi\sigma_0}{\sqrt{2^{-2}3\pi^2 - 4}}\\
&\quad\times\left[1 + \left(\frac{\psi(\mathbf{r}) - k_L d + \arctan x_R^{-1} d}{k_L x_R}\right)^2\right]^{1/2},\\
A(\mathbf{r}) &= \frac{amc\omega_L}{e}\frac{\sqrt{x_R^2+d^2}}{\sqrt{x_R^2+x_0^2}}\frac{\sigma_0}{\sigma(\mathbf{r})}\frac{\pi}{\sqrt{2^{-2}3\pi^2-4}},
\end{aligned}
\tag{6}
$$

where $a = 500$ is the laser pulse amplitude, $\sigma_x = 8\sqrt{2\pi}\lambda$ is the pulse length, $d = 12\lambda$ is the distance from the center of the last pulse to the gas-volume center, $x_R = \pi\sigma_0^2/\lambda$, $\sigma_0 = 3\lambda$, and $k_L = 2\pi/\lambda$. The other components of the electric and magnetic fields at $t = 0$ can be calculated from Maxwell's equations $\nabla\cdot\mathbf{E} = \nabla\cdot\mathbf{B} = 0$.

The gas density is chosen to be less than 10^{16} cm $^{-3}$ so that the collisional effects (collisional ionization, bremsstrahlung, pair photoproduction by nuclei, etc.) can be neglected (see discussion in Sec. IV). The seed electrons for cascade triggering are produced by the field ionization of the gas atoms. Noble gases He, Ne, Ar, Kr, and Xe are explored. In order to study the contribution of the electrons bound in the different atom shells the densities of the gases are chosen to be inversely proportional to the atomic numbers, so that the number of electrons produced after full ionization is the same for all gases. For example, the density of He is 9.03×10^{15} cm^{-3} in our simulations, which is in 27 times higher than the density of Xe, 3.35×10^{14} cm^{-3}. Therefore, in the case of full atom ionization the densities of the ionization-produced electrons for both gases are the same.

First, we study QED cascade development in He. The gas volume in the simulation has a length of 40λ along the x axis ($8\lambda \leqslant x \leqslant 48\lambda$) and 5λ along the y axis ($14\lambda \leqslant y \leqslant 19\lambda$) and the z axis ($14\lambda \leqslant z \leqslant 19\lambda$). Further enlargement of the gas volume in all directions does not increase the number of pairs produced in the cascades (see Fig. 4). The gas density is 9.03×10^{15} cm^{-3}.

The distributions of the electrons, positrons, ions, and E_y are shown in Fig. 5 at different moments of time. The pulse centers cross each other in $x = 28\lambda$ at $t = 18\lambda/c$. The counterpropagating laser pulses generate a field structure

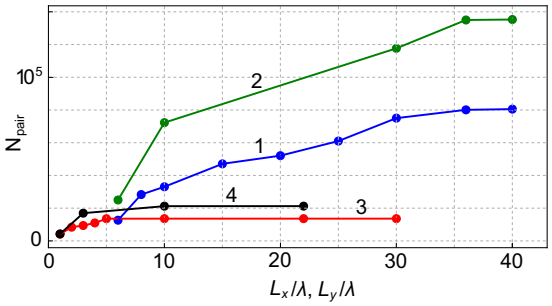

FIG. 4. The number of pairs produced in the cascade as a function of the gas-volume length (along the x axis, L_x) for He (line 1) and for Xe (line 2) as well as a function of the gas-volume width (along y and z axes, $L_y = L_z$) for He (line 3) and for Xe (line 4).

which is close to the linearly polarized standing wave near $x = 28\lambda$. In the case of He the full ionization of atoms occurs already at the laser pulse front. For $t \geqslant 10\lambda/c$ the gas is fully ionized, and new electrons are not produced due to field ionization. Most of the produced electrons are pushed out by the ponderomotive force of the laser pulse from the high-intensity region in the transverse direction and cannot

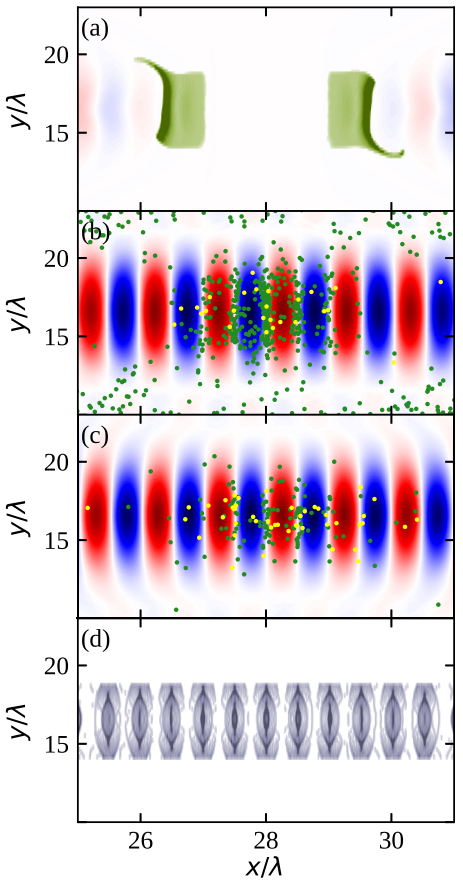

FIG. 5. The distribution of the electrons (green dots), the positrons (yellow dots), and the laser field component E_y (blue and red shading) in the x-y plane at (a) $t = 8\lambda/c$, (b) $t = 15\lambda/c$, and (c) $t = 18\lambda/c$ for He. (d) The distribution of the He ions in the x-y plane at $t = 18\lambda/c$.

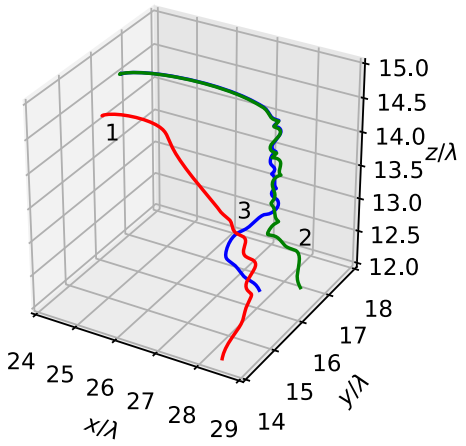

FIG. 6. The trajectory of the escaping electrons pushed out by the ponderomotive force from the high-intensity region (line 1) and the trajectory of the trapped electrons staying for a long time in the region, where laser field peaks (lines 2 and 3). The electrons are created by ionization of He atoms.

initiate cascade. A small portion of the electrons moves along with the laser pulses, thereby forming two counterpropagating relativistic bunches [see Fig. 5(a)]. The motion of each bunch is stopped by the counterpropagating laser pulse. Moreover, the bunch electrons are trapped in the standing-wave nodes corresponding to the minimum of the ponderomotive potential [see Fig. 5(b)] [12,35,36].

The typical trajectories of the trapped electrons staying for a long time in the region where the laser field peaks ($x = 28\lambda$, $y = 16.5\lambda$, $z = 16.5\lambda$) and the escaping electrons are pushed out by the ponderomotive force from the high-intensity region are shown in Fig. 6. When the wave strength becomes strong enough, the bunched electrons start to initiate cascade with prolific pair production. It follows from the simulations that the pairs are efficiently produced within time interval $12\lambda/c \leqslant t \leqslant 23\lambda/c$. The ion density also peaks in the wave nodes [see Fig. 5(d)].

The density of Xe in the simulations is $3.35 \times 10^{14}\,\mathrm{cm}^{-3}$, which is in 27 times less than the density of He, so that the number of the atomic electrons in the gas volume is the same for both gases. The cascade development in Xe is shown in Fig. 6. Like for He, the small portion of electrons produced from outer shell of Xe atoms in the laser pulse fronts forms counterpropagating bunches [see Fig. 7(a)]. The bunched electrons are trapped in the nodes of the standing wave generated near $x = 28\lambda$, where the laser pulse centers cross each other [see Fig. 7(b)].

In contrast to He the electrons are still produced by field ionization of Xe even after laser pulse crossing ($t \geqslant 18\lambda/c$) because the ionization potential of the inner-shell electrons of the Xe atom is about 3 orders of magnitude higher than that of He. Typical trajectories of the $2s^1$ electrons of Xe are shown in Fig. 8. It is seen that some inner-shell electrons escape from the high-intensity region, while the other inner-shell electrons undergo oscillations in the strong laser field for a long time and emit high-energy photons. It follows from Fig. 7 that, like for He, the densities of the electrons, positrons, and ions also peak

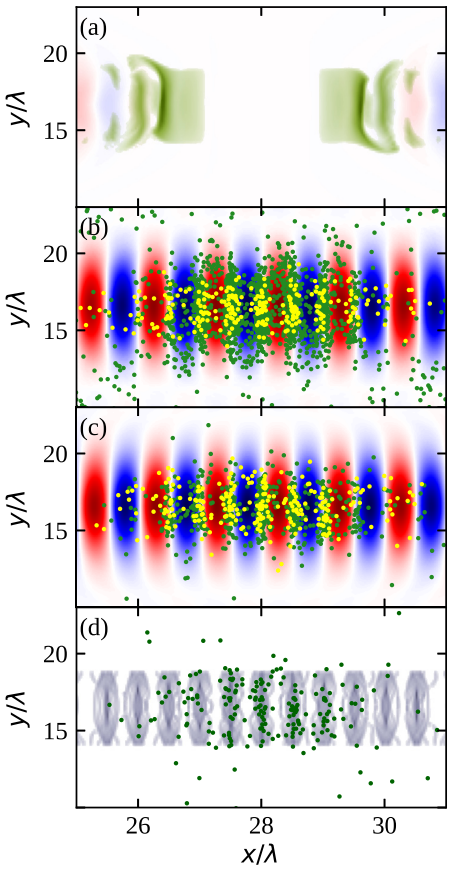

FIG. 7. The distribution of the electrons (green dots), the positrons (yellow dots), and the laser field component E_y (blue and red shading) in the x-y plane at (a) $t = 8\lambda/c$, (b) $t = 15\lambda/c$, and (c) $t = 18\lambda/c$ for Xe. (d) The distribution of the inner-shell ($2s^1$) electrons (green dots) and Xe ions (gray shading) in the x-y plane at $t = 18\lambda/c$.

in the nodes of the standing wave forming near the volume center.

The dynamics of the inner-shell electron population and of the high-charge ion population are shown in Fig. 9. Figure 9 illustrates that the ions with the highest charges Xe $^{+52}$ are produced when the laser pulses cross and the laser field strength peaks. The ionization production rate for the inner-shell electrons and the positron production rate are significant at $7\lambda/c < t < 22\lambda/c$ when the laser field is strong. Therefore the cascade in Xe can be initiated not only by the outer-shell electrons trapped in the standing wave but also by the inner-shell electrons produced when the laser field becomes strong enough for cascade development.

The pair numbers as a function of time in all noble gases are shown in Fig. 10. The gas densities are normalized to the atomic numbers so that the electron densities in the case of full atom ionization are the same for all gases. The gas densities of He, Ne, Ar, Kr, and Xe are 9.03×10^{15}, 1.81×10^{15}, 10^{15}, 5.02×10^{14}, and $3.34 \times 10^{14}\,\mathrm{cm}^{-3}$, respectively. The gas volume has a length of $5\lambda/c$ and a width of $5\lambda/c$. It is seen from Fig. 4 that the ratio $N_p(\mathrm{Xe})/N_p(\mathrm{He})$ remains nearly unchanged with increasing volume size. Thus we can expect that the ratio of the positron numbers presented in Fig. 10 for

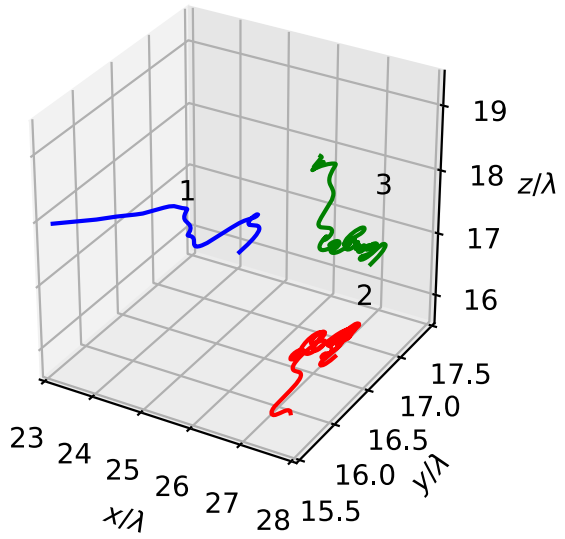

FIG. 8. The trajectories of the escaping inner-shell ($2s^1$) electrons of Xe (line 1) and the inner-shell electrons of Xe (lines 2 and 3) staying for a long time in the region, where the laser field peaks.

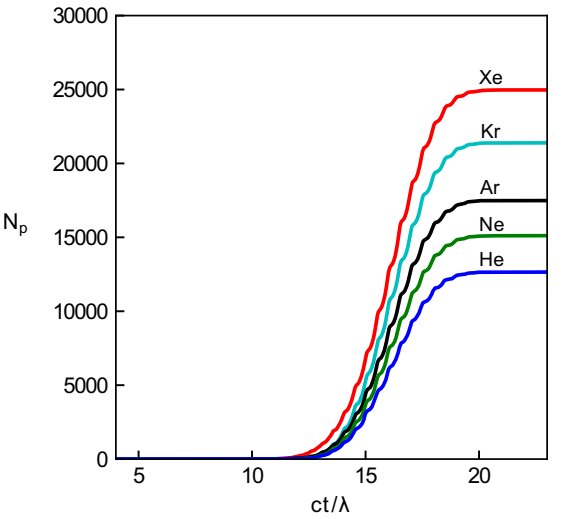

FIG. 10. The pair number as a function of time for He, Ne, Ar, Kr, and Xe.

the noble gases will be similar for a macroscopic gas target ($L \gg 40\lambda/c$). Despite the fact that Xe density is 27 times less than He density, the number of pairs produced in Xe is about 2 times larger than that in He. Therefore the inner-shell electrons play an important role in QED cascade triggering. The spectra of the electrons and photons produced in the cascade in He and Xe are shown in Fig. 11. The energy of the particles is slightly higher in Xe than in He.

IV. DISCUSSIONS AND CONCLUSIONS

A simple formula for the field-ionization rate covering the whole range of laser intensity was proposed. The formula is based on a combination of known expressions for tunnel ionization in the low-intensity limit [16,17,21,23] and the ionization-rate formula in the extremely intense limit, where the rate is proportional to the strength of the electric field. The linear dependence on the field strength is in qualitative agreement with numerical TDSE calculations for hydrogen [28] if $E \gg E_{cr}$. However, more detailed validation of the proposed formula is needed.

QED cascades in noble gases were studied. It was shown that there are two main mechanisms of seed electron production and cascade initiation in high-Z gases like Ar, Kr, and Xe: (i) the ionization of the outer-shell electrons moving along with the pulses to the cascade region and (ii) the ionization of the inner-shell electrons created at the time instant when the pulses cross and the total laser field peaks. The ionization

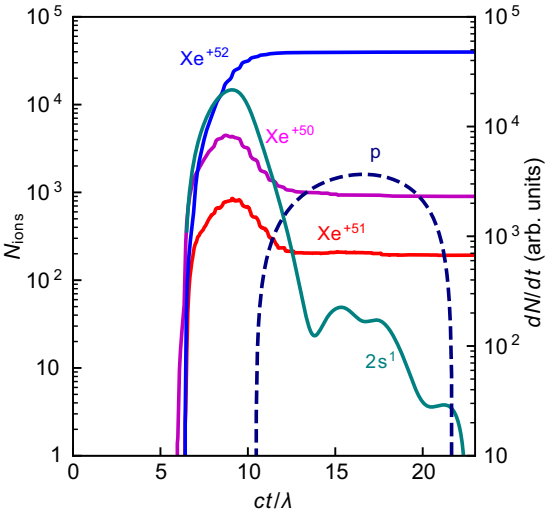

FIG. 9. The number of high-charge ions, the ionization production rate for the inner-shell electrons, and the positron production rate as a function of time in Xe.

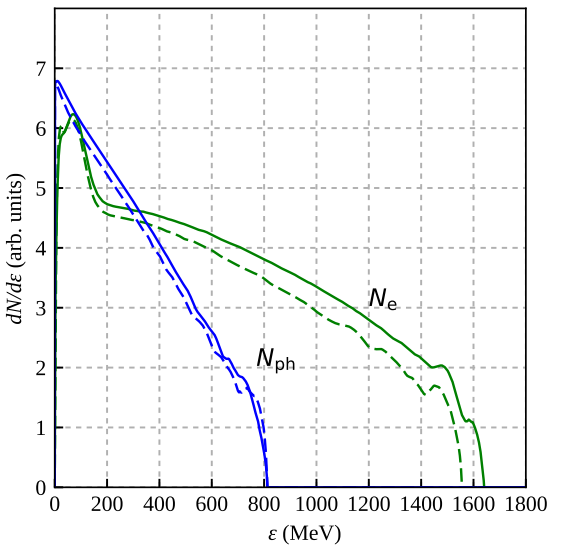

FIG. 11. The spectrum of the photons in He (dashed blue line) and in Xe (solid blue line) and the spectrum of the electrons in He (dashed green line) and in Xe (solid green line) at $t = 28\lambda/c$.

potentials of $2s^1$ and $2s^2$ electrons of Xe are about 10 keV. Those electrons can escape from the ion only at very high field strength. In low-Z gases like He and Ne, only the first mechanism is possible. These gases are fully ionized in the laser pulse front. Most of the electrons are pushed out by the ponderomotive force of the laser pulse from the high-intensity region and cannot initiate cascade. A small portion of the produced electrons may move along with the laser pulses up to the time instance when the pulses cross and the laser field becomes strong enough for cascading.

The first mechanism is discussed in Ref. [12], where electron trapping in the cascade region is observed in numerical simulations. It was demonstrated that some of the seed electrons survive up to pulse crossing and are trapped near the electric-field nodes of the standing wave formed by the counterpropagating pulses. The second mechanism is discussed in Ref. [7], where ionization is included in cascade simulations. However, the ionization model was too simple and does not take into account the probabilistic nature of ionization and sequential multiple ionizations of electrons from different shells of high-Z atoms. Moreover, all atom electrons leave the atom simultaneously according to this model. We use in our simulations a more realistic model providing a probabilistic description of field ionization. This model allows us to analyze the role of both mechanisms. It follows from our simulations that in high-Z gases like Ar, Kr, and Xe both mechanisms are important for cascade initialization: the outer-shell electrons are involved in the first mechanism, while the inner-shell electrons are involved in the second one. Comparing pair production in He and Xe (see Figs. 4 and 10), we can conclude that the inner-shell electrons of Xe increase pair production about 2 times for the parameters of interest despite the fact that Xe density is 27 times less than He density. The result is obtained when the peak laser field strength $2a = 1000$ is close to the cascade threshold value. With increasing laser intensity the role of the mechanisms can be changed.

QED cascade develops as a result of chain reactions when photon emission caused by electron scattering in the laser field (Compton scattering) alternates with pair photoproduction due to photon scattering in the laser field (Breit-Wheeler process). However, high-energy photons and pairs can also be produced by collisional processes neglected in our numerical simulations. Photons can be emitted at electron scattering by ionic or atomic nuclei (bremsstrahlung), while pairs can be created by a high-energy photon interacting with ionic or atomic nuclei. First, we estimate the bremsstrahlung contribution to the cascade. The total bremsstrahlung cross section in the limit $\varepsilon_e \gg \varepsilon_e' \gg m_e c_e^2$ is $\sigma_{br} = (2^{5/2}/3)Z^2\alpha r_e^2 \gamma_e^{1/2}$, where ε_e and ε_e' are the electron energies before and after scattering by an ion, respectively, $\gamma_e = \varepsilon_e/(m_e c^2)$ is the relativistic gamma factor of the electron, $\alpha = e^2/(c\hbar) \approx 1/137$ is the fine-structure constant, and $r_e = e^2/(m_e c^2) \simeq 2.82 \times 10^{-13}$ cm is the classic radius of the electron [37]. The number of bremsstrahlung photons can be estimated as follows: $N_{bph} \simeq n_e N_i c\sigma_{br}\tau_c$, where n_e is the density of the relativistic electrons, N_i is the number of ions in the cascade volume, and τ_c is the cascade duration. According to the simulation, the cascade volume is $V_c \sim 5\lambda \times 5\lambda \times 5\lambda$, and the cascade duration is $\tau_c \simeq 7\lambda/c$ (see Fig. 9). For full ionization of the xenon gas with $Z = 54$ and $n_g = 3.34 \times 10^{14}$ cm^{-3} we obtain $n_e = Zn_g \simeq 1.8 \times 10^{16}$ cm^{-3}, $N_i = n_g V_c \simeq 4.18 \times 10^4$, and $N_{bph} \simeq 9.51 \times 10^{-5}$, where the mean gamma factor of the electron $\gamma_e \simeq 10^3$ is used. It follows from estimation that the number of bremsstrahlung photons is negligible with the number of cascade photons ($N_{ph} > 10^5$).

The number of electron-positron pairs produced by the high-energy photons near nuclei can be estimated as follows: $N_{npair} \simeq n_{ph} N_i c\sigma_{npair}\tau_c$, where $\sigma_{br} \simeq (28/9)Z^2\alpha r_e^2[\ln(2\varepsilon_{ph}/m_e c^2) - (109/42) - 1.2(\alpha Z)^2]$ is the cross section of pair production near nuclei in the relativistic limit ($\varepsilon_{e,ph} \gg m_e c^2$) and $n_{ph} = N_{ph}/V_c$ is the photon density in the cascade volume [37]. It follows from the simulations that the number of high-energy photons ($\varepsilon_{ph} > 1$ MeV) is less than $N_{ph} < 10^6$; therefore the number of pairs produced by photons near nuclei is $N_{npair} < 10^{-5}$, which is much less than the pair number produced in the cascade $N_{pair} > 10^4$.

The contribution of the collisional ionization can also be estimated in a similar way. The cross section of the collisional ionization for the relativistic electrons is $\sigma_{ci} \simeq (2^{7/2}\pi^{1/2}/3)Z^2\alpha r_e^2 L$, where L is the Coulomb logarithm [38]. Even for a very large value of $L = 20$ the number of electrons produced via collisional ionization $N_{e,ci} = n_e N_i c\sigma_{ci}\tau_c \simeq 0.016$ is much less than the number of electrons created via field ionization $N_e \gg N_i > 10^4$ in the cascade volume. Thus collision ionization can be neglected in the cascade modeling.

The electrons can also be produced by the collision of high-energy photons with atoms or partially ionized ions (photoelectric effect). This effect of one-photon ionization is not included in our numerical scheme for field ionization. The photoelectric cross section peaks for photons with energy $\varepsilon_{ph} < m_e c^2$ and does not exceed $\sigma_{phe} < 10^{-19}$ cm^{-2} [39]. It follows from Fig. 11 that the mean energy of the cascade photons is more than 100 MeV and photons with energy $\varepsilon_{ph} < m_e c^2$ belong to the low-energy part of the photon spectra. The number of photons radiated by the electron moving in the laser field per unit time can be estimated as follows: $dN_{ph}/d\varepsilon_{ph} = \varepsilon_{ph}^{-1} dI/d\varepsilon_{ph}$ and $dN_{ph}/d\varepsilon_{ph} \simeq \omega_L^{-1} 0.021\alpha a_S \chi_e^{2/3}\gamma_e^{-4/3}(\varepsilon_{ph}/m_e c^2)^{-2/3}$, where the approximation for the low-energy part of the synchrotron radiation spectrum is used, $dI/d\varepsilon_{ph}$ is the synchrotron radiation spectrum [40], and $a_S = m_e c^2/\hbar\omega_L$. The number of low-energy photons emitted during cascade development is $N_{ph}(\varepsilon_{ph} < m_e c^2) \simeq 0.063\alpha a_S \chi_e^{2/3}\gamma_e^{-4/3}(\omega_L\tau_c) \simeq 4$, where $\chi_e \simeq 10$ is taken from the simulations. The number of electrons produced via the photoelectric effect in the cascade region during cascade development is $N_{e,phe} = (N_{ph}/V_c)N_i c\sigma_{phe}\tau_c \simeq 10^{-7}$, which is much less than the number of electrons created via field ionization $N_e \gg N_i > 10^4$. Therefore the photoelectric effect can also be neglected in the cascade modeling. The losses associated with the ionization are also neglected in the simulations because the ionization energy ($<0.1 m_e c^2$) is several order of magnitude less than the mean electron energy in the laser field ($\sim 10^3 m_e c^2$).

Finally, it was demonstrated Xe among noble gases is more appropriate for facilitating QED cascading. However,

the additional effects like the laser pulse propagation from the focusing parabolas to the cascade volume, the accurate description of the gas target, and ionization dynamics should be taken into account for realistic simulations of possible laboratory experiments.

ACKNOWLEDGMENTS

This work was supported in part by "Basis" Foundation Grant No. 17-11-101-1. The numerical simulations of QED cascades were supported by Russian Science Foundation Grant No. 16-12-10383.

[1] A. R. Bell and J. G. Kirk, Phys. Rev. Lett. **101**, 200403 (2008).
[2] A. Di Piazza, C. Müller, K. Z. Hatsagortsyan, and C. H. Keitel, Rev. Mod. Phys. **84**, 1177 (2012).
[3] N. B. Narozhnyi and A. M. Fedotov, Phys. Usp. **58**, 95 (2015).
[4] N. P. Zafir, Eur. Phys. J. Spec. Top. **223**, 1221 (2014).
[5] J. P. Zou, C. Le Blanc, D. N. Papadopoulos, G. Cheriaux, P. Georges, G. Mennerat, F. Druon, L. Lecherbourg, A. Pellegrina, P. Ramirez, F. Giambruno, A. Freneaux, F. Leconte, D. Badarau, J. M. Boudenne, D. Fournet, T. Valloton, J. L. Paillard, J. L. Veray, M. Pina, P. Monot, J. P. Chambaret, P. Martin, F. Mathieu, P. Audebert, and F. Amiranoff, High Power Laser Sci. Eng. **3**, e2 (2015).
[6] E. G. Gelfer, A. A. Mironov, A. M. Fedotov, V. F. Bashmakov, E. N. Nerush, I. Yu. Kostyukov, and N. B. Narozhny, Phys. Rev. A **92**, 022113 (2015).
[7] M. Tamburini, A. Di Piazza, and C. H. Keitel, Sci. Rep. **7**, 5694 (2017).
[8] A. Gonoskov, A. Bashinov, S. Bastrakov, E. Efimenko, A. Ilderton, A. Kim, M. Marklund, I. Meyerov, A. Muraviev, and A. Sergeev, arXiv:1610.06404.
[9] G. Breit and J. A. Wheeler, Phys. Rev. **46**, 1087 (1934).
[10] A. M. Fedotov, N. B. Narozhny, G. Mourou, and G. Korn, Phys. Rev. Lett. **105**, 080402 (2010).
[11] E. N. Nerush, I. Yu. Kostyukov, A. M. Fedotov, N. B. Narozhny, N. V. Elkina, and H. Ruhl, Phys. Rev. Lett. **106**, 035001 (2011).
[12] M. Jirka, O. Klimo, S. V. Bulanov, T. Zh. Esirkepov, E. Gelfer, S. S. Bulanov, S. Weber, and G. Korn, Phys. Rev. E **93**, 023207 (2016).
[13] I. Gonoskov, A. Aiello, S. Heugel, and G. Leuchs, Phys. Rev. A **86**, 053836 (2012).
[14] E. N. Nerush and I. Yu. Kostyukov, Nucl. Instrum. Methods Phys. Res., Sect. A **653**, 7 (2011).
[15] A. A. Mironov, A. M. Fedotov, and N. B. Narozhnyi, Quantum Electron. **46**, 305 (2016).
[16] A. M. Perelomov, V. S. Popov, and M. V. Terent'ev, Zh. Eksp. Teor. Fiz. **50**, 1393 (1966) [Sov. Phys. JETP **23**, 924 (1966)].
[17] V. S. Popov, Phys. Usp. **47**, 855 (2015).
[18] I. I. Artemenko, A. A. Golovanov, I. Yu. Kostyukov, T. M. Kukushkina, V. S. Lebedev, E. N. Nerush, A. S. Samsonov, and D. A. Serebryakov, JETP Lett. **104**, 883 (2016).
[19] L. V. Keldysh, Zh. Eksp. Teor. Fiz. **47**, 1945 (1964) [Sov. Phys. JETP **20**, 1307 (1965)].
[20] F. A. Ilkov, J. E. Decker, and S. L. Chin, J . Phys. B **25**, 405 (1992).
[21] B. M. Karnakov, V. D. Mur, S. V. Popruzhenko, and V. S. Popov, Phys. Usp. **58**, 3 (2015).
[22] *Handbook of Mathematical Functions*, edited by M. Abramowitz and I. A. Stegun (Dover, New York, 1972).
[23] M. V. Ammosov, N. B. Delone, and V. P. Kraĭnov, Zh. Eksp. Teor. Fiz. **91**, 2008 (1986) [Sov. Phys. JETP **64**, 1191 (1986)].
[24] N. B. Delone and V. P. Krainov, Phys. Usp. **42**, 669 (1999).
[25] D. Bauer, Phys. Rev. A **55**, 2180 (1997).
[26] X. M. Tong and C. D. Lin, J. Phys. B **38**, 2593 (2005).
[27] V. P. Krainov, J. Opt. Soc. Am. B **14**, 425 (1997).
[28] D. Bauer and P. Mulser, Phys. Rev. A **59**, 569 (1999).
[29] Q. Zhang, P. Lan, and P. Lu, Phys. Rev. A **90**, 043410 (2014).
[30] R. Nuter, L. Gremillet, E. Lefebvre, A. Levy, T. Ceccotti, and P. Martin, Phys. Plasmas **18**, 033107 (2011).
[31] S. C. Rae and K. Burnett, Phys. Rev. A **46**, 1084 (1992).
[32] M. Chen, E. Cormier-Michel, C. G. R. Geddes, D. L. Bruhwiler, L. L. Yu, E. Esarey, C. B. Schroeder, and W. P. Leemans, J. Comput. Phys. **236**, 220 (2013).
[33] A. V. Korzhimanov, E. S. Efimenko, A. V. Kim, and S. V. Golubev, Quantum Electron. **43**, 217 (2013).
[34] E. N. Nerush and I. Yu. Kostyukov, Probl. Atom. Sci. Tech. **4**, 3 (2010).
[35] G. Lehmann and K. H. Spatschek, Phys. Rev. E **85**, 056412 (2012).
[36] A. Gonoskov, A. Bashinov, I. Gonoskov, C. Harvey, A. Ilderton, A. Kim, M. Marklund, G. Mourou, and A. Sergeev, Phys. Rev. Lett. **113**, 014801 (2014).
[37] V. B. Berestetskii, E. M. Lifshits, and L. P. Pitaevskii, *Quantum Electrodynamics* (Pergamon, New York, 1982).
[38] D. Wu, X. T. He, W. Yu, and S. Fritzsche, arXiv:1703.05127.
[39] E. Storm and H. I. Israel, Nucl. Data Tables **A7**, 565 (1970).
[40] V. N. Baier, V. M. Katkov, and V. M. Strakhovenko, *Electromagnetic Processes at High Energies in Oriented Single Crystals* (World Scientific, Singapore, 1998).